

15 Abstract

16 The solar tides of the mesosphere and lower thermosphere (MLT) show great vari-
 17 ability on timescales of days to years, with significant variability at interannual timescales.
 18 However, the nature and causes of this variability remain poorly understood. Here, we
 19 present measurements made over the interval 2005 to 2020 of the interannual variabil-
 20 ity of the 12-hour tide as measured at heights of 80 to 100 km by a meteor radar over
 21 Rothera (68° S, 68° W). We use a linear regression analysis to investigate correlations
 22 between the 12-hour tidal amplitudes and several climate indices, specifically the solar
 23 cycle (as measured by F10.7 solar flux), El Niño Southern Oscillation (ENSO), the Quasi-
 24 Biennial Oscillation (QBO) at 10 hPa and 30 hPa and the Southern Annular Mode (SAM).
 25 Our observations reveal that the 12-hour tide has a large amplitude and a clearly defined
 26 seasonal cycle with monthly mean values as large as 35 ms⁻¹. We observe substantial
 27 interannual variability, exhibiting 2σ range in monthly mean 12-hour tidal amplitudes
 28 at the height of 95 km in spring of 13.4 ms⁻¹, 11.2 ms⁻¹ in summer, 18.6 ms⁻¹ in au-
 29 tumn and 7.0 ms⁻¹ in winter. We find that F10.7, QBO10, QBO30, SAM and time all
 30 have significant correlations to the 12-hour tidal amplitudes at the 95% level, with a lin-
 31 ear trend also present. Whereas we detect very minimal correlation with ENSO. These
 32 results suggest that variations in F10.7, the QBO and SAM may contribute significantly
 33 to the interannual variability of 12-hour tidal amplitudes in the Antarctic MLT.

34 1 Introduction

35 In the mesosphere and lower thermosphere (MLT), at heights of 80 to 100 km, the
 36 wind field is dominated by the global scale oscillations of the solar atmospheric tides.
 37 These tides can reach very large amplitudes of several 10s of ms⁻¹ and can be critical
 38 to the dynamics and coupling of the whole atmosphere. These tides are primarily ex-
 39 cited by the solar heating of ozone and water vapour in the stratosphere and troposphere,
 40 the release of latent heat in deep tropospheric convection, and/or non-linear interactions
 41 involving tides and planetary waves (Vadas et al., 2014; Hagan & Forbes, 2002).

42 The tides are apparent in many different atmospheric variables, including wind, tem-
 43 perature and density. They are often the most prominent features of the wind field of
 44 the MLT. Consequently, they can have a profound impact on the coupling and dynam-
 45 ics of the atmosphere. For example, tidal winds can filter the field of atmospheric grav-
 46 ity waves (C. L. Beldon & Mitchell, 2010). This filtering controls the propagation of grav-
 47 ity waves to greater heights, thus modulating gravity-wave momentum fluxes and the
 48 resulting forcing of the global atmospheric circulation (Fritts & Alexander, 2003; Yiğit
 49 et al., 2021). In addition to wind perturbations, tidal temperature perturbations can also
 50 play an important role and are thought to be a driver of the variability of polar meso-
 51 spheric clouds, modulating the cloud ice crystal population (Fiedler et al., 2005).

52 Tides can propagate upwards from the MLT, higher into the upper thermosphere
 53 where they may affect neutral and plasma concentrations in the ionosphere’s E and F
 54 regions, modulating the ionospheric wind dynamo (Yiğit & Medvedev, 2015; H.-L. Liu,
 55 2016; Sobhkhiz-Miandehi et al., 2022). They can also alter the total electron content (TEC)
 56 of the ionosphere, influencing the conditions for seeding equatorial plasma bubbles in the
 57 F-region (Oberheide et al., 2009; Immel et al., 2006). These important features mean
 58 that understanding the tides is vital to understanding the dynamics and coupling of at-
 59 mospheric layers (Smith, 2012).

60 Observations of MLT winds reveal large amplitude tides with periods which are har-
 61 monics of the solar day (Chapman & Lindzen, 1970). At middle and polar latitudes the
 62 largest amplitudes are observed in the 12-hour tide, with the 24- and 8-hour tides hav-
 63 ing significantly smaller amplitudes (Dempsey et al., 2021; Davis et al., 2013). The dom-
 64 inance of the 12-hour tide at polar latitudes means that determining the climatology and

variability of this tide is particularly important in studies of the polar atmosphere. Consequently, a number of observational studies have attempted to determine the climatology and variability of the 12-hour tide at polar latitudes, including (N. J. Mitchell, 2002; Conte et al., 2017; Dempsey et al., 2021). Here, our focus is on the 12-hour tide alone and we will not further consider the 24- or 8-hour tides.

The polar 12-hour tide in the MLT is known to display a distinct seasonal variability with maximum amplitudes generally occurring at heights above 90 km in the autumn months of April - May with a secondary maximum occurring at similar heights in August - September (N. J. Mitchell, 2002; Dempsey et al., 2021). Beyond this, the polar 12-hour tide is also observed to display significant inter-annual variability with changes in amplitude of several ms^{-1} occurring from year to year (Conte et al., 2017). These latter variations in amplitude have been proposed to be linked to external drivers that modify the excitation and/or propagation of the tide. Potential drivers of interannual variability at polar and other latitudes include:

- solar variability (e.g. Namboothiri et al. (1993); Bremer et al. (1997); C. Beldon et al. (2006); Guharay et al. (2019); Nischal et al. (2019)),
- the El Niño Southern Oscillation (ENSO) (e.g., Lieberman et al. (2007); Pedatella and Liu (2012); H. Liu et al. (2017); Sundararajan (2020) amongst others),
- and the stratospheric Quasi-Biennial Oscillation (QBO) (e.g., Hibbins et al. (2007); Forbes et al. (2008); Pancheva et al. (2009); Hibbins et al. (2010); Laskar et al. (2016)).

We should also note that in addition to this inter-annual variability, the 12-hour tide displays great short-term variability on time scales ranging from a few days to several months. In addition, short-term tides also respond to the QBO, ENSO and solar cycle (see Dhadly et al. (2018); Vitharana et al. (2019); Kumari and Oberheide (2020)) Here, however, we will consider only the inter-annual variability.

We will now consider the above potential drivers of inter-annual variability in the polar 12-hour tide in more detail.

Variations in solar flux are an obvious potential driver of variability because the migrating component of tides are strongly excited by the solar heating of ozone and water vapour in the troposphere and stratosphere and the temperature structure of the atmosphere through which the tide must propagate may similarly change. A negative correlation between F10.7 solar flux and tidal amplitudes has been reported by (Sprenger & Schminder, 1969; Namboothiri et al., 1993; Bremer et al., 1997). At polar latitudes, Baumgaertner et al. (2005) investigated the relationship between solar flux and Antarctic 12-hour tidal amplitudes measured at Scott Base (78°S , 167°E) using an MF radar and discovered a negative correlation between solar F10.7 flux and tidal amplitudes. These authors also noted a positive trend in tidal amplitudes which they suggested may be a consequence of increased cooling of the atmosphere produced by a rise in CO_2 resulting in pressure and density decreases in the MLT. This would increase tidal amplitudes at a particular height given that the gas density at this height would be decreased.

ENSO causes large-scale changes in tropospheric convection (K. E. Trenberth, 2002; Lieberman et al., 2007). These changes may modify tidal forcing in the troposphere, resulting in corresponding tidal variability in the MLT. Zonal mean winds in the stratosphere and mesosphere are also believed to be influenced by ENSO (Sassi, 2004) and thus may modulate tidal amplitudes in the global MLT by changing the propagation environment for the tide (Pedatella & Liu, 2012).

QBO signatures have been found in 12-hour MLT tides in a number of studies. For example at mid-latitudes, Forbes et al. (2008) found QBO modulations of $\pm 10 - 15\%$ in 12-hour tidal amplitudes. They proposed that this was due to modulation by the QBO

115 as the tides propagate upwards from their tropospheric and stratospheric source regions
 116 into the MLT. Pancheva et al. (2009) investigated temperature tides using data from Sound-
 117 ing of the Atmosphere using Broadband Emission Radiometry (SABER) and winds from
 118 the TIMED Doppler Interferometer (TIDI) onboard the Thermosphere Ionosphere Meso-
 119 sphere Energetics and Dynamics (TIMED) satellite and reported QBO modulation of
 120 the migrating 12-hour tidal amplitude at mid-latitudes in both hemispheres. At polar
 121 latitudes, Hibbins et al. (2007, 2010) used the SuperDARN radar located at Halley, Antarc-
 122 tica (76°S, 27°W) to measure meteor winds in both the zonal and meridional compo-
 123 nents and observed a large QBO modulation of the summertime 12-hour non-migrating
 124 tide. Laskar et al. (2016) investigated the 12-hour tide at 69°N, a conjugate latitude to
 125 our study, using meteor-radar observations and Modern Era-Retrospective Analysis for
 126 Research and Applications (MERRA) winds and reported that variations in the enhance-
 127 ment of the tidal amplitudes during August to September are linked to low-latitude QBO
 128 winds.

129 The SAM describes the north/south movement of the belt of eastward winds centred
 130 at 50/55° latitude (Marshall, 2003). It substantially impacts the climatic systems
 131 of the southern hemisphere’s high and mid-latitudes and influences climate variability
 132 and change in the southern hemisphere. The surface zonal winds of SAM and the south-
 133 ern hemisphere greatly impact the tropospheric and oceanic circulation systems (Lee et
 134 al., 2019; Abram et al., 2014). However, there have been very few studies of the links
 135 between the SAM and MLT winds and tides. Merzlyakov et al. (2009) investigated MLT
 136 wind and tide measurements from a meteor radar situated at Molodezhnaya (67.7°S, 45.9°E)
 137 and MF radars at Mawson (67.6°S, 62.9°E) and Davis (68.6°S, 78.0°E). They found no
 138 significant link between SAM and the MLT. In contrast, Noble et al. (2022) found a cor-
 139 relation between the SAM and MLT winds measured by meteor radar at Rothera, in the
 140 same dataset as considered in our study. It is possible that the SAM modulation of MLT
 141 winds could impact MLT tidal amplitudes.

142 In this study, we use meteor radar observations of zonal and meridional winds in
 143 the Antarctic MLT made at Rothera (68°S, 68°W) to measure the amplitude of the 12-
 144 hour tide. We determine its seasonal variability and its interannual variability. We then
 145 use a linear regression model to identify any correlations between the interannual vari-
 146 ability of monthly estimates of tidal amplitude and indices representing climate processes.
 147 The model includes terms that represent the following potential drivers of tidal variabil-
 148 ity:

- 149 1. Solar variability as measured by the F10.7 Solar flux
- 150 2. The El Nino Southern Oscillation (ENSO)
- 151 3. The Quasi-Biennial Oscillation (QBO)
- 152 4. The Southern Annual Mode (SAM).

153 The meteor radar at Rothera is an ideal instrument for this type of study because it is
 154 able to make robust measurements of tidal amplitude at heights of 80 - 100 km over ex-
 155 tended intervals. Here we use observations made over the interval 2005 to 2020, form-
 156 ing one of the longest records of polar MLT winds available.

157 In Section 2, we describe the radar, data and the climate indices we have used. Sec-
 158 tion 3, describes the methods used to obtain estimates of monthly tidal amplitudes from
 159 hourly winds and the linear regression analysis used to extract the time-series correla-
 160 tion of the tidal amplitudes and the climate indices. In Section 4, we present the results
 161 of our analysis. In Section 5, we consider our results compared to other studies linking
 162 tidal amplitudes in the MLT and climate indices. Finally, in Section 6, we present our
 163 conclusions.

2 Data

2.1 Meteor Radar

Meteor radar have been used in many ground-based tidal studies (e.g. Stober, Kuchar, et al. (2021); Dempsey et al. (2021); Davis et al. (2013); C. Beldon et al. (2006); N. J. Mitchell (2002)) and is a well established method of measuring MLT winds from 75 to 105 km. Using inferred winds from meteor trails, meteor radars are able to determine tidal amplitudes, wavelengths, and variability at a variety of scales, such as small-scale gravity waves with periods less than 2 hours, horizontal wavelength less than 400 km and vertical wavelengths up to 3–5 km (Song et al., 2021); They have also been used to investigate planetary waves, such as the interaction between the 12-hour tide and the 16-day planetary wave (Mthembu et al., 2013; Day et al., 2012). They are ideally suited to investigating MLT tidal amplitudes which become large at these heights. As such, meteor radars are well-suited to study polar interannual tidal variability.

We are using tidal amplitudes obtained from hourly winds measured in the MLT by a SKiYMET VHF meteor radar located at Rothera (68°S, 68°W) from 1st January 2005 to 31st December 2020. Hourly winds are estimated using the radial velocity measurements taken from each individual meteor, assuming that the flow is horizontal and uniform across the meteor collecting volume at any given height. We calculate the winds by combining the inferred horizontal velocities obtained for each meteor with a Gaussian weighting in height and time around a specific height and specific time. The full-width-half-maxima for these Gaussian weightings are 2 h in time and 3 km in height. The centre of the Gaussian progresses across the data in 1 h time and 1 km height steps, giving hourly winds between 75 - 105 km (Hindley et al., 2021).

The Rothera radar employs a solid-state transmitter with a peak power of 6 kW and was installed in 2005. In 2019, the antennae were replaced following weather-related degradation. This reduced the fraction of ambiguous meteors detected.

The radar antenna receiver array uses five interferometer elements to measure echo azimuth and zenith angles. When combined with range data, this allows the height of individual meteor echoes to be determined. In practice, this allows us to determine MLT winds down to approximately 2 h in time and 2 km in space (N. Mitchell & Beldon, 2009). The meteor radar installed at Rothera (68°S, 68°W) has been used in numerous studies for investigating MLT winds (D. J. Sandford et al., 2010), atmospheric tides (Dempsey et al., 2021; C. L. Beldon & Mitchell, 2010; D. Sandford et al., 2007), planetary waves (Mthembu et al., 2013) and gravity waves (N. Mitchell & Beldon, 2009; C. Beldon & Mitchell, 2009). For a detailed overview of the Rothera meteor radar, see N. Mitchell and Beldon (2009). Note, as we only use one radar in this study, we are unable to separate migrating (sun-following, westward propagating) and non-migrating modes (not sun-following), and observe a superposition of both. For a detailed description of general SKiYMET radar operation see Hocking et al. (2001). Due to an increased spread of meteor height distribution at certain periods over the dataset, the following days have been removed: January 2005, December 2009, January 2010, December 2010, the entirety of 2016 to 2018.

2.2 Time Series of Climate Indices

To qualify the dependence of tidal amplitudes on specific climate indices, we regress monthly values of five climate indices and time against 12-hour tidal amplitudes. These indices are F10.7 solar flux, ENSO, QBO10, QBO30 and SAM.

For solar flux, we use the observed solar flux F10.7 index, defined as the solar radio flux at 10.7 cm radio emission measured on the surface of Earth. It is one of the longest-running records of solar activity, and so we can use it as an indicator of solar activity

212 in our linear regression. It is measured in solar flux units (SFU), with 1 SFU equal to
 213 $10^{-22} \text{ W m}^{-2} \text{ Hz}^{-1}$ and provided by the National Research Council of Canada.

214 For the El Niño Southern Oscillation, we use the Niño 3.4 index, representing the
 215 average equatorial sea surface temperature (SST) anomalies (measured in kelvin) in a
 216 box bound by $5^{\circ}\text{N} - 5^{\circ}\text{S}$, $170^{\circ}\text{W} - 120^{\circ}\text{W}$. This index uses a 5-month running mean, and
 217 the El Niño or La Niña events are defined when the Niño 3.4 SST anomalies exceed \pm
 218 0.4 K for six months or more (K. Trenberth, 2018).

219 For the Quasi Biennial Oscillation (QBO) indices, the ERA5 zonal mean zonal wind
 220 (in ms^{-1}) is averaged over 5°N to 5°S at 10 hPa for the QBO10 index and at 30 hPa for
 221 the QBO30 index. These two heights were chosen to capture possible QBO responses
 222 because they are almost orthogonal to each other (Chiodo et al., 2014) (please see Fig-
 223 ure S1).

224 For the Southern Annular mode, we use the Marshall Southern Annular Mode in-
 225 dex (SAM index) which is the difference between the normalised monthly zonal sea level
 226 pressure (SLP) at 40°S minus the normalised monthly zonal sea level pressure at 65°S .
 227 Six stations are used to calculate a proxy zonal mean sea level pressure at both 40° and
 228 65°S (Marshall, 2003, 2018).

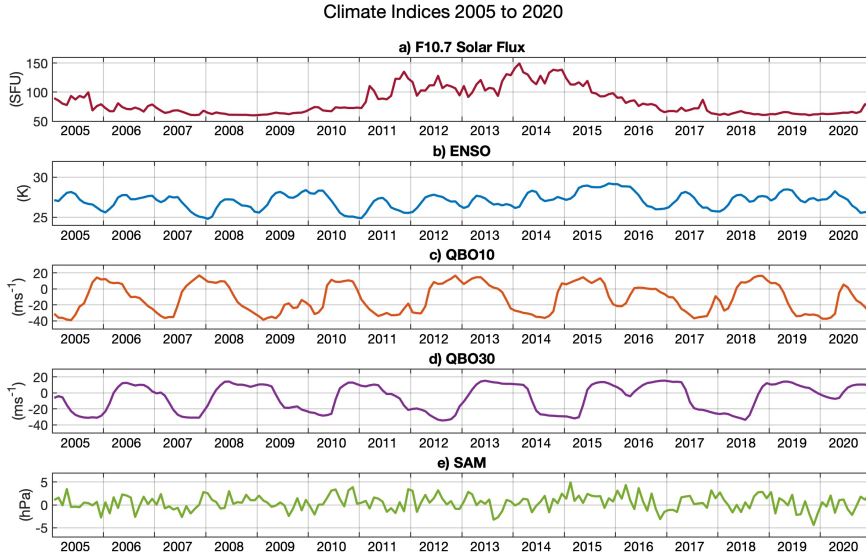


Figure 1: Time-series of the global climate indices of (a) F10.7 Solar Flux, (b) ENSO, (c) QBO10, (d) QBO30 and (e) SAM for the period 2005 to 2020.

229 Figure 1 presents the time series of the five climate indices over the 2005 to 2020
 230 period. Our chosen period encompasses the entirety of solar cycle 24, which has a min-
 231 imum in December 2008 and the following minimum in December 2019, shown in Fig-
 232 ure 1a. In Figure 1b, the ENSO index varies systematically from 25 K to 29 K but with-
 233 out a strongly-fixed period. The QBO10 index in Figure 1c has a more defined period,
 234 with a regular period of around 22 months. This is similar to the QBO30 (in Figure 1d)
 235 index which has a similar period but lagged by around 9 months from the QBO10 in-
 236 dex (for a Lomb-Scargle periodogram of these two indices, please see Figure S2). Finally,
 237 in Figure 1e, the SAM index does not have a strong periodicity and no apparent trend.

238

2.2.1 Inclusion of an Ozone Term

239

240

241

242

243

244

245

246

247

248

One driver for atmospheric tides is the solar excitation of ozone in the stratosphere. It would therefore make sense to use an index representing ozone in our linear regression. However, the inclusion of this term in our model would cause it to be unstable due to correlations with ENSO and also time, i.e. the presence of a linear trend (for a complete table of the correlation of the climate indices against the other indices used in the study, please see Table S1). Therefore, to investigate any potential links with ENSO, we have decided to omit the ozone term. This is consistent with Pancheva et al. (2003) who found that ozone can be used as a proxy for planetary wave activity. As we are considering an absorption term with the inclusion of F10.7 solar flux, we are not proceeding with any ozone term in our linear model.

249

3 Method

250

3.1 Tidal Amplitudes from Hourly Winds

251

252

253

254

255

256

257

To investigate the interannual variability of the tides in the mesosphere and lower thermosphere, we calculate amplitudes of the 12-hour tide using meteor radar hourly winds over the time period 2005 to 2020. We obtain tidal amplitudes by creating a monthly composite day of the winds and fitting sinusoidal waves of tidal periods to the composite day at each height. These have periods of 24, 12, 8 and 6 hours. For more detail, see Dempsey et al. (2021). We will be using only the 12-hour tide for this study, as this tide has the largest amplitude at this latitude.

258

3.2 Linear Regression

259

260

261

262

We will now explain our linear regression analysis of the 12-hour tidal amplitudes. Similarly to Gan et al. (2017) and Ramesh et al. (2020), we begin with the tidal anomaly. This is defined as the deviation of each month from the climatological mean. This step is to remove the seasonal cycle.

263

264

265

266

267

268

To build a multilinear regression model for each month, we separate our data and use a three-month window centred on the month of interest. The linear regression analysis is performed independently on each height level for the meridional and zonal tidal amplitudes. We propose and implement the following linear regression model, and we estimate the unknown parameters using the Ordinary Least Squares (OLS) method. We use the following expression for the linear model:

$$A'_{12} = \beta_0 + (\beta_1 F10.7) + (\beta_2 ENSO) + (\beta_3 QBO10) + (\beta_4 QBO30) + (\beta_5 SAM) + (\beta_6 Time) \quad (1)$$

269

270

where A'_{12} is the 12-hour tidal amplitude minus the seasonality, β_0 is the constant and β_1 to β_6 are the coefficients of the climate variables.

271

272

273

274

275

276

277

278

279

280

Linear regression is a robust technique for finding correlations between variables, and it allows us to deconstruct the tidal anomaly into component portions that can be attributed to various external factors. However, correlation does not always imply causality; hence, a correlation between tidal amplitudes and indices could be purely coincidental rather than causal. There are likely to be other causes of interannual variability besides the indices we regress against, but it is impossible to include everything without overcomplicating our model. Therefore, we must interpret the results with caution when employing linear regression. Treated carefully, these findings allow us to investigate linear impacts of atmospheric and solar oscillations on tidal amplitudes in the Antarctic MLT.

281

3.2.1 Multicollinearity

282

283

284

285

286

287

For the linear regression to be valid, we need to check that there is no multicollinearity, that is, that none of the indices used are correlated with each other. The presence of multicollinearity means variables are correlated. If that were the case, then the results from our linear regression would be unreliable. This test ensures solar flux, ENSO, QBO10, QBO30, SAM, and time are independent of each other. We test this by calculating Variance Inflation Factors (VIFs).

288

289

VIFs are created by firstly regressing each independent variable against the others and then calculating the VIF as follows:

$$VIF = \frac{1}{(1 - R^2)} \quad (2)$$

290

291

292

293

294

295

296

297

where R^2 is the R-squared value. The values of the VIF range from 1 to infinity, with values around 1 suggesting that there is no multicollinearity; values between 1 and 5 suggesting some multicollinearity, but not enough to disrupt the model; values over 5 suggesting correlation and are cause for concern; and values over 10 are a major problem and imply a strong correlation (Kalnins, 2018). For our linear regression, the VIFs range from 1.02 to 1.35. As our values are around 1, the variables we have chosen to explain tidal amplitude variability do not suffer from multicollinearity, and therefore, we can use them confidently.

298

3.2.2 Auto-correlation

299

300

301

302

To perform a linear regression, the residuals must be free from auto-correlation, which means the residuals from the linear regression are not correlated with each other. Auto-correlation would indicate that essential information is missing from the model and that we cannot rely on the standard errors.

303

304

305

306

307

308

309

To determine the presence of auto-correlation, we use the Durbin-Watson (DW) test which yields a test statistic to detect autocorrelation in the residuals from a regression analysis. It returns a number between 0 and 4 (Webster, 2012). A score of 2 indicates no auto-correlation, whereas results closer to 0 indicate positive auto-correlation, and results closer to 4 indicate negative auto-correlation. In the current study, we use the definition that readings between 1.5 and 2.5 are normal and results below 1 and above 3 indicate some form of auto-correlation (Webster, 2012).

310

311

312

313

Because we create many models to describe the tidal amplitudes, we have many DW statistics. The meteor radar tidal amplitude DW statistics all lie in the acceptable 1 to 3 range, with 86% falling in the 1.5 to 2.5 acceptable range. Therefore, our DW results all fall within the acceptable range.

314

4 Results

315

4.1 12-hour Tidal Amplitudes

316

317

318

319

320

321

Figure 2 presents the zonal and meridional tidal amplitudes at 95 km and 90 km from 2005 to 2020. In Figure 2a to d, each pixel represents the monthly tidal amplitude given by the year on the y-axis with the month given on the x-. All of these plots have the same scale for comparison to each other. In Figure 2e to h, line plots of the mean amplitude over the year with the inter-quartile range of the monthly amplitudes plotted in purple and the extreme values in grey shading.

322

323

324

In each panel there is considerable interannual variability. Each month exhibits a range of amplitudes over 2005 to 2020. For example, at 90 km the month of May typically has the largest amplitudes in each year and exhibits a substantial variability in mea-

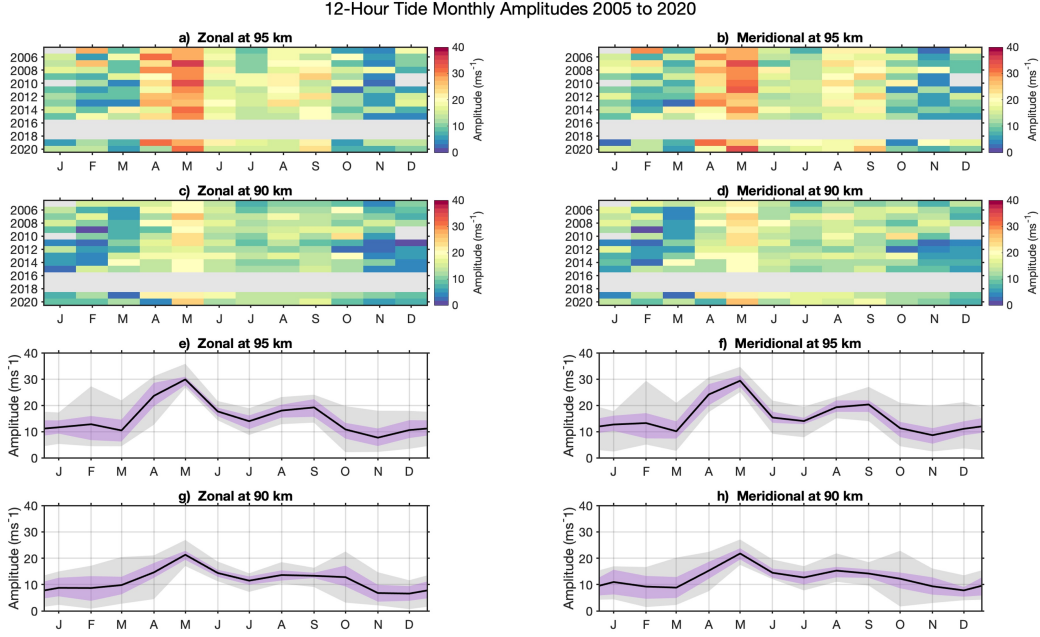


Figure 2: Monthly 12-hour tidal amplitudes for the period 2005 to 2020 for (a) zonal tidal amplitudes at 95 km, (b) meridional tidal amplitudes at 95 km, (c) zonal tidal amplitudes at 90 km, (d) meridional tidal amplitudes at 90 km, where each coloured pixel represents the monthly tidal amplitude. The grey bars indicate where data has been removed due to quality issues. The line plots represent the average monthly tidal amplitudes, with the interquartile range of each month in purple shading and the extreme values in grey for the (e) zonal monthly 12-hour tidal amplitudes at 95 km, (f) meridional at 95 km, (g) zonal at 90 km and (h) meridional at 90 km.

325 sured amplitude across the years. May also has the largest amplitudes at 95 km, reach-
 326 ing 35 ms^{-1} , seen in Figure 2a and b. In panels a and b, every month exhibits consid-
 327 erable variability between years. For 95 km, the 2σ range in monthly mean 12-hour tidal
 328 amplitudes is 13.4 ms^{-1} in spring, 11.2 ms^{-1} in summer, 18.6 ms^{-1} in autumn and 7.0
 329 ms^{-1} in winter. At 90 km, in Figure 2c, we can see May 2007 exhibits an amplitude of
 330 27 ms^{-1} , whereas in 2012, the month of May exhibits an amplitude of 15 ms^{-1} . In Fig-
 331 ures 2c and d, we can see that in December (during austral summer) at 90 km, there is
 332 a large decrease in amplitudes from 2011 to 2015. At 95 km, in Figures 2a and b, this
 333 is not repeated. In Figure 2e to h we present line plots indicating the mean average of
 334 tidal amplitudes across the year with the interquartile range in purple and the extreme
 335 values in grey. We can see from these plots that, especially at 95 km, the tidal ampli-
 336 tudes demonstrate considerable differences in each month. This is especially clear in Febru-
 337 ary and November in panels e and f. Given the large spread in amplitudes for each month,
 338 there is enough evidence to proceed with our investigation.

339 4.1.1 Average Year 12-hour Tide

340 We can also calculate an average year for our data set, shown in Figure 3. Figure
 341 3a and b present the monthly tidal amplitude averaged over the 15 years for the zonal
 342 and meridional components, respectively. In the zonal component, we can see that there
 343 are two peaks in amplitude in the year, representing the semi-annual cycle in tidal ampli-
 344 tudes peaking close to the equinoxes. In April, the first peak reaches amplitudes \sim
 345 40 ms^{-1} above 95 km, sustaining until mid-May. The second peak occurs in August but

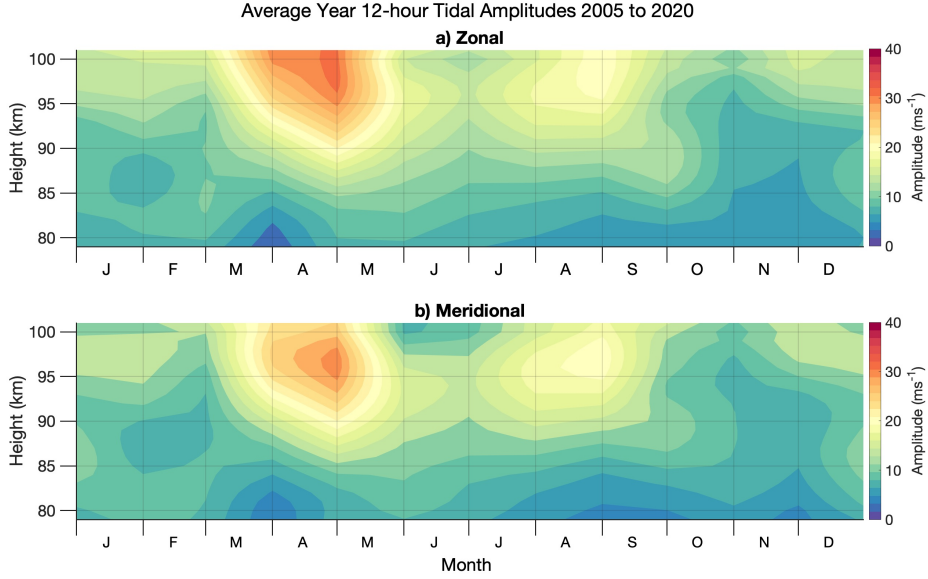


Figure 3: Average year 12-hour tidal amplitudes over the height range 80 to 100 km for the period 2005 to 2020 for (a) zonal and (b) meridional components.

346 with a smaller amplitude of around 24 ms^{-1} . The smallest tidal amplitudes are found
 347 near 80 km in height towards the end of March and early April, where tidal amplitudes
 348 are near 3 ms^{-1} . In general, examples of larger amplitudes exist between March and Septem-
 349 ber above 90 km, whereas examples of smaller values exist between October and Febru-
 350 ary especially near 80 km. For the meridional component in Figure 3b, the tidal ampli-
 351 tudes display a semi-annual cycle with two peaks in amplitude in April and late August.
 352 These peaks occur at a similar height and again close to the equinoxes, as in the zonal.

353 4.2 Correlation of Climate Variables to Interannual Tidal Variability

354 Next, we explore the result of our linear regression analysis on the polar 12-hour
 355 tidal amplitudes from the meteor radar. As we have performed the linear regression anal-
 356 ysis on the zonal and meridional components of the polar 12-hour tide, we have two plots
 357 for each index. Here, we present time-height contours of the coefficients from the linear
 358 regression analysis for each climate index, as given in Equation 1, e.g. β_1 to β_6 . Each
 359 result is plotted as a time-height contour plot, with positive values corresponding to an
 360 increase in amplitude represented by red shading and negative values corresponding to
 361 a decrease in amplitude by blue shading. For each plot, we have overlaid contours rep-
 362 resenting the significance level using t-test statistics (from a two-tailed student's t-test),
 363 with the dashed contour representing the 80% confidence level and the solid contour in-
 364 dicated the 90% significance level. We will therefore only discuss correlations with 90%
 365 significance. In all of the indices used in this study, we use response to suggest a link be-
 366 tween the index being studied and the variability of the 12-hour tidal amplitude in the
 367 MLT. We note that correlations do not inherently imply causation, we use them here as
 368 a guide to the causal mechanisms at play.

369 We have scaled the colour bar axis using the difference between the 90th and 10th
 370 percentile of each index, hereafter defined as the interdecile range, α . Table 1 presents
 371 these values for each index. We use α to give a comparable scale for each index so we

372 may compare the relative correlations. As α is calculated using the climate index, it is
 373 the same regardless of tidal component.

Index	Interdecile range (α)
F10.7 Solar Flux	57.6 SFU
ENSO	2.67 K
QBO10	45.8 ms ⁻¹
QBO30	42.8 ms ⁻¹
SAM	4.02 hPa

Table 1: The interdecile range, α , used to scale the linear regression response plots (Figures 4 to 9) for each given index.

374 **4.2.1 Solar Flux**

375 In Figure 4 we present the results for F10.7 solar flux from the linear regression anal-
 376 ysis of the 12-hour tidal amplitudes, i.e. the solar coefficient of the linear model β_1 . The
 377 most noticeable feature in both the zonal (Figure 4a) and the meridional (Figure 4b) is
 378 the large negative response at the beginning of the year and at the end of the year, be-
 379 tween 85 and 93 km, where we see a response of up to -4 ms⁻¹ per α SFU solar flux (where
 380 $\alpha = 57.6$ SFU). The meridional component also has a large statistically-significant re-
 381 gion in mid-June, extending through December and into February at a large range of heights.
 382 In the middle of the year, this response is -3 ms⁻¹ per α SFU in June at 90 km, grow-
 383 ing to -4 ms⁻¹ per α SFU at 90 km in December.

384 **4.2.2 ENSO**

385 The results of the response of polar 12-hour tidal amplitudes to El Niño Southern
 386 Oscillation ENSO are presented in Figure 5a and b in the zonal and meridional compo-
 387 nents, respectively. ENSO does not present many significant regions compared to the other
 388 indices used in this study. The only notable feature in both components is a small sig-
 389 nificant region below 82 km in height from late February to April with a response of -2
 390 ms⁻¹ per α K, where $\alpha = 2.67$ K. As there are not any further significant regions, we
 391 are unable to make any further correlations with the polar 12-hour tide.

392 **4.2.3 QBO at 10 hPa**

393 The results for the response of the polar 12-hour tide to the QBO10 index are pre-
 394 sented in Figure 6a and b for the zonal and meridional components, respectively. The
 395 most striking feature in this Figure is a strong negative response of -5 ms⁻¹ per α ms⁻¹
 396 QBO10 from December to January at most heights (where $\alpha = 45.8$ ms⁻¹ QBO10). This
 397 feature is also found in the zonal component but is weaker. Both components also have
 398 significant responses in the middle of the year. In the zonal component, this is seen from
 399 May to June centred at 95 km with a 4 ms⁻¹ per α ms⁻¹ QBO10 response and in the
 400 meridional, we see a -3 ms⁻¹ per α ms⁻¹ QBO10 response from June to July centred
 401 at 95 km.

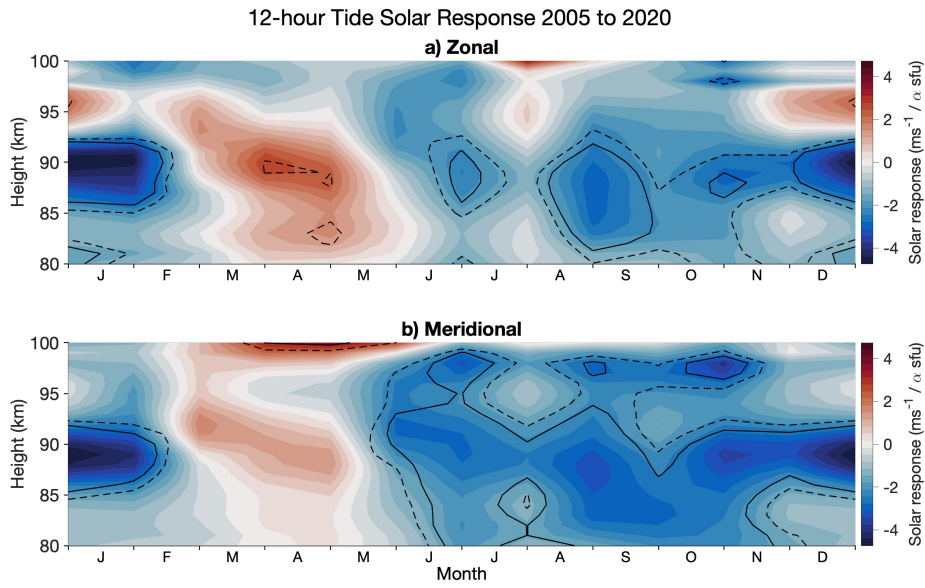


Figure 4: 12-hour tide F10.7 Solar Flux response to tidal amplitudes over the height range 80 to 100 km for the period 2005 to 2020, for the (a) zonal and (b) meridional components. Dashed and solid contours indicate the 80% and 90% confidence intervals, respectively, according to the t-test.

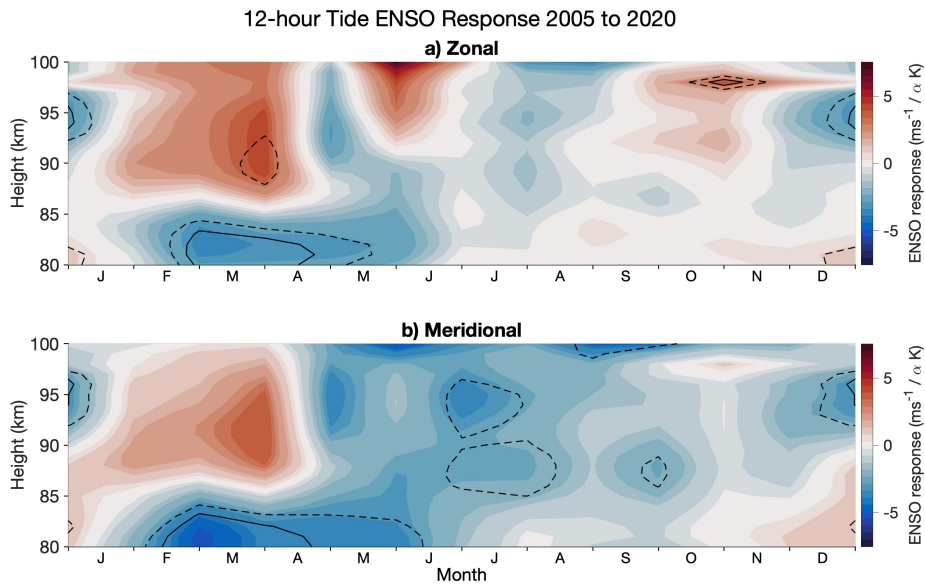


Figure 5: 12-hour tide ENSO response to tidal amplitudes over the height range 80 to 100 km for the period 2005 to 2020, for the (a) zonal and (b) meridional components. Dashed and solid contours indicate the 80% and 90% confidence intervals, respectively, according to the t-test.

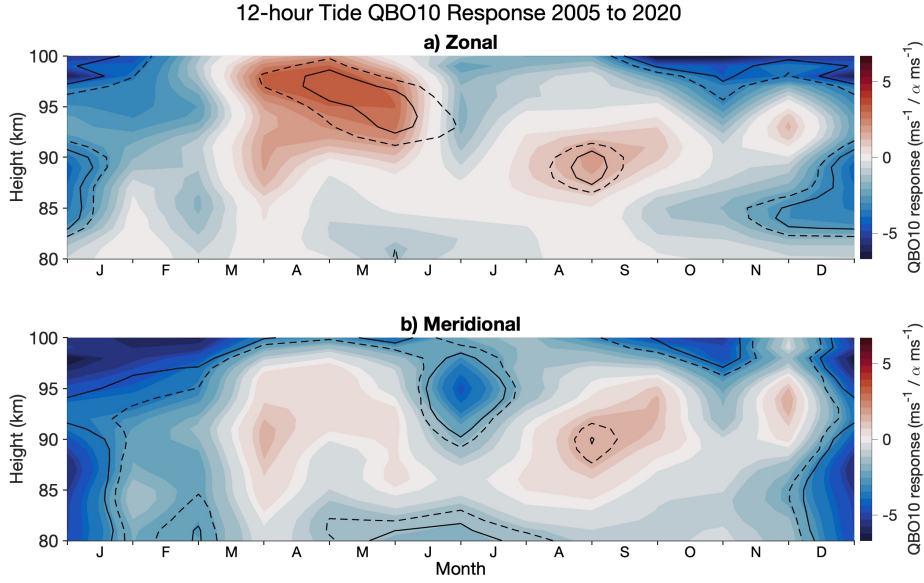


Figure 6: 12-hour tide QBO10 response to tidal amplitudes over the height range 80 to 100 km for the period 2005 to 2020, for the (a) zonal and (b) meridional components. Dashed and solid contours indicate the 80% and 90% confidence intervals, respectively, according to the t-test.

402

4.2.4 QBO at 30 hPa

403

404

405

406

407

408

409

410

411

412

413

The results for the response of the polar 12-hour tide to the QBO30 index are presented in Figure 7a and b for the zonal and meridional component, respectively. In the zonal component, Figure 7a, there are instances of significance across the year. The most noticeable instance is from May to June, where there is a weak positive response of 3 ms^{-1} per $\alpha \text{ ms}^{-1}$ QBO30 below 90 km. In November, there is a further significant region beginning at 4 ms^{-1} per $\alpha \text{ ms}^{-1}$ QBO30 and extending through to January, becoming a negative response of -2 ms^{-1} per $\alpha \text{ ms}^{-1}$ QBO30. The QBO30 index in the meridional, Figure 7b, exhibits a strong negative response in January of -6 ms^{-1} per $\alpha \text{ ms}^{-1}$ QBO30 above 95 km and -4 ms^{-1} per $\alpha \text{ ms}^{-1}$ QBO30 below 90 km during January (where $\alpha = 42.8 \text{ ms}^{-1}$). Unlike QBO10, this feature is not reflected in the zonal component in Figure 7a.

414

4.2.5 SAM

415

416

417

418

419

420

421

The results for the response of the polar 12-hour tide to the SAM index are presented in Figure 8a and b for the zonal and meridional component, respectively. In both the zonal and meridional components there are significant regions from December to January above 90 km. This reaches -5 ms^{-1} per $\alpha \text{ hPa SAM}$ (where $\alpha = 4.02 \text{ hPa}$). We also see a positive response in each component in February to April above 95 km. Here we see responses of 5 ms^{-1} per $\alpha \text{ hPa SAM}$. The other regions of significance seen are small and also have a minimal magnitude.

422

4.2.6 Linear Trends

423

424

The results for the presence of linear trends, are presented in Figure 9a and b for the zonal and meridional component, respectively. There is a large significant response

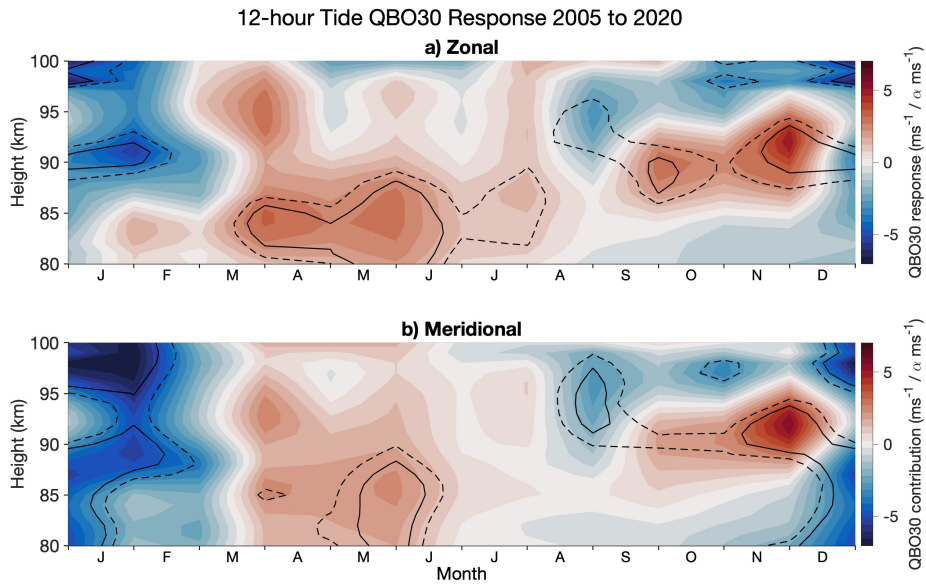


Figure 7: 12-hour tide QBO30 response to tidal amplitudes over the height range 80 to 100 km for the period 2005 to 2020, for the (a) zonal and (b) meridional components. Dashed and solid contours indicate the 80% and 90% confidence intervals, respectively, according to the t-test.

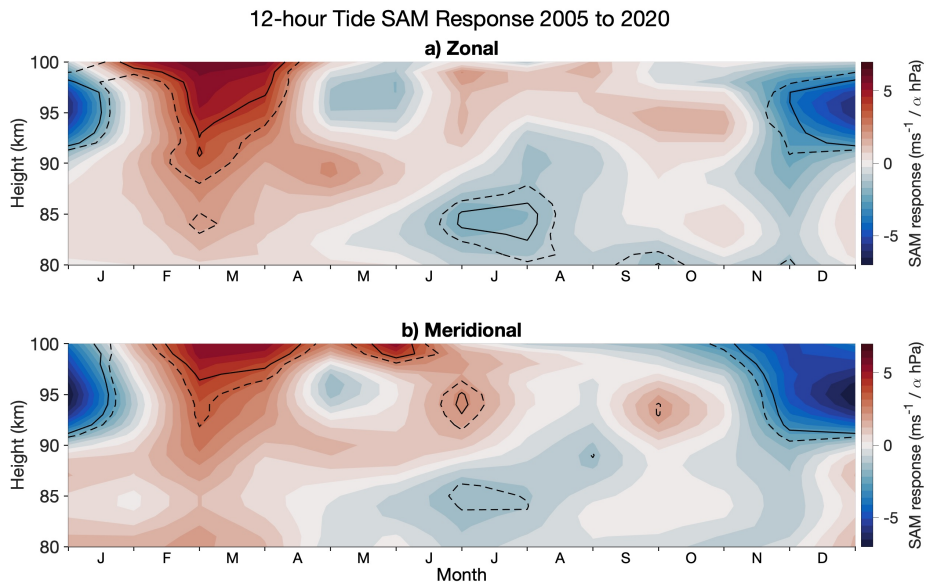


Figure 8: 12-hour tide SAM response to tidal amplitudes over the height range 80 to 100 km for the period 2005 to 2020, for the (a) zonal and (b) meridional components. Dashed and solid contours indicate the 80% and 90% confidence intervals, respectively, according to the t-test.

425 of $-1 \text{ ms}^{-1}/\text{year}$ from February to June above 90 km in the zonal component, Figure 9a.
 426 This is a large response when considering our 15 years of data. We also see small con-
 427 tributions in the meridional component in Figure 9b. For example, in late August, above
 428 87 km, there is a response of $0.2 \text{ ms}^{-1}/\text{year}$. Over 15 years of our dataset, this becomes
 429 3 ms^{-1} . Compared to monthly amplitudes at this time of around 10 to 15 ms^{-1} , the cor-
 430 relations are not to be ignored.

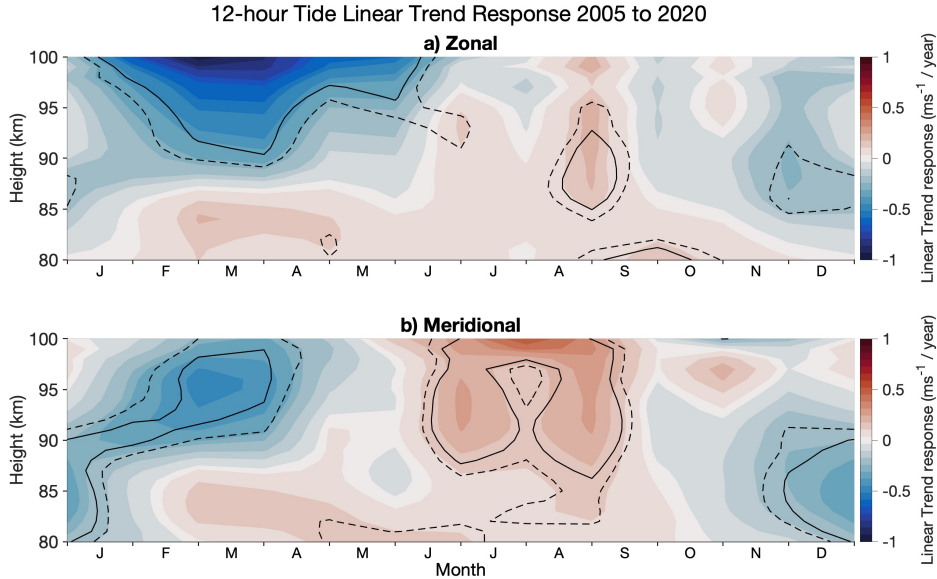


Figure 9: 12-hour tide time response to tidal amplitudes over the height range 80 to 100 km for the period 2005 to 2020, for the (a) zonal and (b) meridional components. Dashed and solid contours indicate the 80% and 90% confidence intervals, respectively, according to the t-test.

431 5 Discussion

432 5.1 Interannual variability

433 We have measured the seasonal climatology and interannual variability of 12-hour
 434 tidal amplitudes in the antarctic MLT and investigated the correlation of this variabil-
 435 ity to climate indices representing solar F10.7 flux, ENSO, QBO10, QBO30, SAM and
 436 time (i.e., linear trends) by performing a linear regression on the 12-hour tidal ampli-
 437 tudes for the period between 2005 and 2020, inclusive. We have found that solar flux,
 438 QBO10, QBO30, SAM and time all have varying degrees of correlation with the ampli-
 439 tudes of the 12-hour tide. In contrast, we have found minimal correlation between ENSO
 440 and the 12-hour tidal amplitudes.

441 In Figure 2, we presented the 12-hour monthly mean tidal amplitudes at 90 and
 442 95 km measured at Rothera. Our analysis reveals a similar seasonal cycle to that reported
 443 in other Antarctic studies, with largest amplitudes occurring in spring and autumn (e.g.,
 444 Stober, Janches, et al. (2021) Dempsey et al. (2021) and C. L. Beldon and Mitchell (2010)).
 445 Further, we found considerable interannual variability in the tidal amplitudes in the MLT.
 446 Such variability appears to be a persistent feature of the polar 12-hour tide and has been
 447 reported in a number of other studies, including Baumgaertner et al. (2005) and Merzlyakov
 448 et al. (2009). Conte et al. (2017) measured the amplitude of the 12-hour tide at Davis

449 (69°S, 78°E) using a meteor radar from 2009 to 2013 and noted less interannual vari-
 450 ability in the winter months and more in summer. Moreover, Baumgaertner et al. (2005)
 451 found that the seasonal behaviour of the 12-hour tide bears a striking resemblance to
 452 the behaviour of planetary wave activity at polar latitudes. They noted that long-term
 453 variations in planetary-wave amplitudes are similar to those of the 12-hour tide and so
 454 proposed that planetary waves may therefore modulate the inter-annual variability of
 455 the tide.

456 Rothera is also host to an MF radar. Hibbins et al. (2007) used data from this MF
 457 radar recorded between 1997 and 2005 to calculate MLT tidal amplitudes and phases.
 458 Note that they did not investigate interannual variability of the tidal amplitudes. They
 459 reported a 12-hour tide with a semi-annual cycle in amplitudes, peaking in April and Septem-
 460 ber - as we observe here. However, we observe significantly larger amplitudes at the up-
 461 per heights with the meteor radar. Further, the tidal amplitudes we present in Figure
 462 2 at 95 km are generally larger than those at 90 km, but this amplitude growth with height
 463 is not apparent in the MF-radar observations of Hibbins et al. (2007). For example, our
 464 results indicate considerable amplitude increases with increasing height over the height
 465 range 90 to 95 km, for example from 22 ms⁻¹ in April 2007 to 33 ms⁻¹ for April 2008.
 466 This is in contrast to the MF-radar observations, which showed approximately constant
 467 amplitudes throughout all heights of around 7 ms⁻¹ with the amplitudes actually de-
 468 creasing slightly at heights above about 95 km. Although made in different years, these
 469 differences are similar to meteor/MF-radar biases reported elsewhere (Manson et al., 2004;
 470 Hines et al., 1993) that have been attributed to properties of the MF radar technique
 471 (Wilhelm et al., 2017).

472 In addition, Conte et al. (2017) measured polar 12-hour tidal amplitudes at Davis
 473 (69°S, 78°E) from 2009 to 2013 and found considerable interannual variability, with sum-
 474 mer demonstrating the most extensive variability. While they found a seasonal cycle, the
 475 timing of this cycle varied with each year. They proposed that the variability seen may
 476 be due to migrating and non-migrating modes, as proposed by Murphy (2003). They found
 477 that between December and February, a westward propagating zonal wave number 1 non-
 478 migrating component dominates the non-migrating tidal contributions to the 12-hour
 479 tide at 68 – 69°S and that between April and October, non-migrating tide activity is very
 480 low, so the westward zonal wave number 2 migrating component dominates. Similarly
 481 to our study, Conte et al. (2017) could not decompose the tidal amplitudes observed as
 482 they used a single station at this latitude.

483 5.2 Correlations between tidal amplitudes and climate indices

484 We have used a linear regression analysis to investigate possible links between the
 485 monthly amplitudes of the antarctic 12-hour tide in the MLT and a number of climate
 486 indices. We have found that solar flux, QBO10, QBO30 and SAM all have at least some
 487 heights and times where there are significant correlations, but that ENSO does not show
 488 significant correlation. We have also found a significant linear trend in the zonal com-
 489 ponent of the 12-hour tidal amplitude response.

490 5.2.1 Solar Flux

491 In Figure 4 we found correlations at the 90% significance level during summer sug-
 492 gesting a -4 ms⁻¹ per α SFU ($\alpha = 57.6$ SFU) relationship in both the zonal and merid-
 493 ional components at heights of 85 to 93 km from December to mid-February. This sig-
 494 nificant region begins in mid-June and extends through to the end of the year in the merid-
 495 ional, where the response becomes strong in December. This implies a negative corre-
 496 lation between F10.7 and the 12-hour tidal amplitude. At antarctic latitudes, Baumgaertner
 497 et al. (2005) investigated the relationship between solar flux and 12-hour tidal amplitudes
 498 at Scott Base (78°S, 167°E) and found a negative correlation between solar activity and

499 12-hour tidal amplitudes at 80 km over the time period 1985 to 2004. Our results thus
 500 reinforce the suggestion that 12-hour tidal amplitudes may decrease, at least in some month,
 501 during times of high solar activity (F10.7). This negative correlation has also been found
 502 at other latitudes (Namboothiri et al., 1993; Bremer et al., 1997).

503 An explanation for the reduction in tidal amplitudes following an increase in solar
 504 flux we observe may lie in the different excitation mechanisms of migrating and non-
 505 migrating tidal modes. The non-migrating modes can be created by non-linear interac-
 506 tions between the migrating modes and planetary waves. However, the migrating modes
 507 are sun following and excited via solar flux (Hagan, 1996; Forbes, 1982). We observe a
 508 superposition of these two modes with the meteor radar. Therefore, an increase in the
 509 amplitude of the migrating mode from the in-situ generation of migrating modes in the
 510 thermosphere via the absorption of extreme UV (Jones et al., 2013; Hagan et al., 2001),
 511 may also increase the non-migrating mode as more interactions can occur (Hagan et al.,
 512 2009; Mayr et al., 2003; McLandress & Ward, 1994). These latter modes may be excited
 513 with a phase that effectively cancels out the migrating mode, reducing the tidal ampli-
 514 tude observed at a particular location.

515 **5.2.2 ENSO**

516 In Figure 5, we found a small significant response between the ENSO index and
 517 monthly 12-hour tidal amplitudes. At equatorial latitudes, H. Liu et al. (2017) simulated
 518 that a ground-based station located south of the equator would detect a substantial en-
 519 hancement of the 24-hour tide in the meridional component during both El Niño and
 520 La Niña but only during El Niño in the zonal component and temperature. Consequently,
 521 there may only be enhancement of the 24-hour tide by ENSO and potentially a reason
 522 why limited significant correlations are found. Our region of significance coincided with
 523 only a small response. Therefore, we can conclude that ENSO shows no extensive sig-
 524 nificant correlation with monthly tidal amplitudes.

525 **5.2.3 QBO**

526 For both the QBO10 and QBO30 indices, Figures 6 and 7 respectively, we have seen
 527 significant correlations. These have been more prominent in the meridional component
 528 in the summertime, where we have seen correlations of -5 ms^{-1} per $\alpha \text{ ms}^{-1}$ QBO10. Be-
 529 tween 1996 and 2004, Hibbins et al. (2007) reported a clear and substantial QBO depen-
 530 dence on the 12-hour tide measured at Halley (76°S , 27°W) with meteor winds from the
 531 SuperDARN radar. The effect was shown to be strongest during the summer months,
 532 with a 2 ms^{-1} decrease in amplitude when the QBO at 35 hPa was positive, and a sim-
 533 ilar rise in amplitude when the QBO at 5 hPa was positive. These findings are consis-
 534 tent as the phase of the QBO changes with increasing equatorial altitude, with the phase
 535 of the QBO recorded at 35 hPa being opposite that of the QBO measured at 5 hPa (Baldwin
 536 & Dunkerton, 1998). Similarly to how we have used the QBO at 10 and 30 hPa. We have
 537 also found a negative correlation during summer months, especially true in the merid-
 538 ional components of the QBO10 and QBO30 tidal amplitude response. Further, (Hibbins
 539 et al., 2010) used 12 years of horizontal wind data from the Scott Base MF radar and
 540 the Halley SuperDARN radar measured between January 1996 and December 2007 to
 541 investigate the migrating ($S = 2$) and non-migrating ($S = 1$) components of the 12-hour
 542 tide around 78°S . They found the amplitude of the summer time $S = 1$ component of
 543 the tide shows a large interannual fluctuation, and a quasi-biennial periodicity is observed
 544 out of phase with the equatorial QBO recorded at 30 hPa. The amplitude and phase of
 545 the migrating $S = 2$ component of the tide show no significant QBO relationship, im-
 546 plying that the previously found QBO dependency on the summer time 12-hour tide at
 547 Halley is only driven by the non-migrating $S = 1$ component.

548

5.2.4 SAM

549

550

551

552

553

554

555

556

557

558

559

560

561

562

We have found that above heights of 90 km, there is a significant correlation from mid-February to mid-April with a positive response of 5 ms^{-1} per α hPa (where $\alpha = 4.02$ hPa). There is then a period of negative response from mid-November to mid-January with a -5 ms^{-1} per α hPa. In contrast, Merzlyakov et al. (2009) sought to identify any correlations between the SAM index and MLT winds and tides and did not find any correlation. They used a meteor radar located at Molodezhnaya (67.7°S , 45.9°E) and MF radars at Mawson (67.6°S , 62.9°E) and Davis (68.6°S , 78.0°E). However, in the current study, we employ a meteor radar with height finding as apposed to a meteor radar without used by Merzlyakov et al. (2009). A system without height finding is unable to determine the growth with height of the tidal amplitudes present in the MLT. Therefore, they observe the average and will miss elements of the tidal amplitude structure. Also MF radars are known to underestimate tidal amplitudes at the upper heights. In combination, this means that in our study, we have been able to use the height finding to our advantage to find a correlation.

563

5.2.5 Linear Trends

564

565

566

567

568

569

570

571

572

573

We have found that there is a significant negative correlation above 95 km from January to May in the zonal component of the tides when investigating linear trends. This suggests that the tidal amplitudes are decreasing with time at this height and period of the year. As mentioned previously, Baumgaertner et al. (2005) found trends in the atmosphere leading to a positive trend in tidal amplitudes and suggested this was due to a rise in atmospheric CO₂ levels causing cooling, resulting in density decreasing more rapidly with height. This would lead to a larger increase of tidal amplitudes with height. This is not something that we observe in the present study. As the strongest linear trend we observe is at the upper heights, indicating that tides are growing to a lesser extent over the years.

574

6 Conclusions

575

576

577

578

579

In this study we have investigated the interannual variability of the tidal amplitudes using a linear regression analysis to identify any links between climate indices and the 12-hour tidal amplitudes in the zonal and meridional components. This study has used a 15 year long data set of 12-hour tidal amplitudes from a meteor radar located at the British Antarctic Survey base at Rothera (68°S , 68°W).

580

We conclude that:

581

582

583

584

585

586

587

588

589

590

591

592

593

594

1. We observe persistent large-amplitude 12-hour tidal amplitudes throughout the period 2005 to 2020 at Rothera, with monthly mean values reaching 13.0 ms^{-1} in spring, 12.0 ms^{-1} in summer, 21.2 ms^{-1} in autumn and 16.4 ms^{-1} in winter.
2. The 12-hour tidal amplitudes show large interannual variability. For example, for 95 km, the 2σ range in monthly mean 12-hour tidal amplitudes is 13.4 ms^{-1} in spring, 11.2 ms^{-1} in summer, 18.6 ms^{-1} in autumn and 7.0 ms^{-1} in winter.
3. The climatological tidal amplitudes we observe are larger than those observed using MF radars at similar latitudes. We propose these differences are due to MF radar bias at the upper heights.
4. Using a linear regression analysis, we find that F10.7 solar flux has a significant negative correlation between tidal amplitudes in both the zonal and meridional component. This is from December to February in both components, with the meridional component showing an additional response from June to November. This strong response has a magnitude of -4 ms^{-1} per α SFU, where $\alpha = 57.6SFU$.

- 595 5. We find that both the QBO10 and QBO30 indices show linear correlations between
 596 the 12-hour tidal amplitudes of the MLT. There is a strong negative correlation
 597 in the meridional component of the tidal amplitude response of the QBO10 and
 598 QBO30 result, with strong responses present in summer at all heights, with the
 599 upper heights having a response of -5 ms^{-1} per $\alpha \text{ ms}^{-1}$ QBO10 ($\alpha = 45.8 \text{ ms}^{-1}$
 600 QBO10) and -6 ms^{-1} per $\alpha \text{ ms}^{-1}$ QBO30 ($\alpha = 42.8 \text{ ms}^{-1}$ QBO30) for the QBO10
 601 and QBO30 indices respectively.
- 602 6. The variation of tidal amplitudes with ENSO is much less significant than the other
 603 indices, suggesting that there is no linear link between ENSO and Antarctic MLT
 604 12-hour tidal amplitudes.
- 605 7. We have identified linear correlations between the SAM and polar 12-hour monthly
 606 tidal amplitudes. We see a positive correlation above 95 km in February to April
 607 whereas we see a negative correlation in November and December above 95 km.
 608 Both are more apparent in the meridional component.
- 609 8. We find that a linear trend is also present in the zonal component of polar 12-hour
 610 tidal amplitude response above 95 km between January and May with a response
 611 of $-1 \text{ ms}^{-1}/\text{year}$.

612 We have shown that the interannual variability of the 12-hour tide is correlated with
 613 several climate indices. Further investigation is needed to understand the mechanisms
 614 behind these potential connections.

615 Data Availability

616 The meteor radar data used in this study is from Mitchell, N. (2019): University of Bath:
 617 Rothera Skiyet Meteor Radar data (2005 – present). Centre for Environmental Data
 618 Analysis, 2022. <https://catalogue.ceda.ac.uk/uuid/aa44e02718fd4ba49cef36d884c6e50>.
 619 The 10.7cm Solar Flux Data are provided as a service by the National Research Coun-
 620 cil of Canada <http://www.spaceweather.ca/solarflux/sx-4-eng.php>.

621 Acknowledgments

622 SMD and PEN are supported by a NERC GW4+ Doctoral Training Partnership stu-
 623 dentship from the Natural Environment Research Council (grant nos. for SMD: NE/L002434/1
 624 and PEN: NE/S007504/1) and are thankful for the support and additional training pro-
 625 vided. TMG, CJW and NJM are supported by the UK Natural Environment Research
 626 Council (grant nos. NE/R001391/1 and NE/R001235/1).

627 CRedit authorship contribution statement

628 Shaun M. Dempsey: Writing - Original draft preparation, Methodology, Software,
 629 Lead Formal Analysis, Investigation, Data Curation. Phoebe E. Noble: Writing - Re-
 630 view, Software, Formal Analysis, Investigation, Data Curation, Validation. Corwin J.
 631 Wright: Supervision, Validation, Writing - Review, Resources. Nicholas J. Mitchell: Su-
 632 pervision, Methodology, Conceptualisation, Resources. Tracy Moffat-Griffin: Supervi-
 633 sion, Writing - Review and Editing, Validation, Resources.

634 References

- 635 Abram, N. J., Mulvaney, R., Vimeux, F., Phipps, S. J., Turner, J., & England,
 636 M. H. (2014, May). Evolution of the southern annular mode during the
 637 past millennium. *Nature Climate Change*, 4(7), 564–569. Retrieved from
 638 <https://doi.org/10.1038/nclimate2235> doi: 10.1038/nclimate2235
 639 Baldwin, M. P., & Dunkerton, T. J. (1998, September). Quasi-biennial modulation
 640 of the southern hemisphere stratospheric polar vortex. *Geophysical Research*

- 641 *Letters*, 25(17), 3343–3346. Retrieved from <https://doi.org/10.1029/98gl02445> doi: 10.1029/98gl02445
- 642
- 643 Baumgaertner, A., McDonald, A., Fraser, G., & Plank, G. (2005, November). Long-term observations of mean winds and tides in the upper mesosphere and lower thermosphere above scott base, antarctica. *Journal of Atmospheric and Solar-Terrestrial Physics*, 67(16), 1480–1496. Retrieved from <https://doi.org/10.1016/j.jastp.2005.07.018> doi: 10.1016/j.jastp.2005.07.018
- 644
- 645
- 646
- 647
- 648 Beldon, C., & Mitchell, N. (2009, June). Gravity waves in the mesopause region observed by meteor radar, 2: Climatologies of gravity waves in the antarctic and arctic. *Journal of Atmospheric and Solar-Terrestrial Physics*, 71(8–9), 875–884. Retrieved from <https://doi.org/10.1016/j.jastp.2009.03.009> doi: 10.1016/j.jastp.2009.03.009
- 649
- 650
- 651
- 652
- 653 Beldon, C., Muller, H., & Mitchell, N. (2006, March). The 8-hour tide in the mesosphere and lower thermosphere over the UK, 1988–2004. *Journal of Atmospheric and Solar-Terrestrial Physics*, 68(6), 655–668. Retrieved from <https://doi.org/10.1016/j.jastp.2005.10.004> doi: 10.1016/j.jastp.2005.10.004
- 654
- 655
- 656
- 657
- 658 Beldon, C. L., & Mitchell, N. J. (2010, September). Gravity wave–tidal interactions in the mesosphere and lower thermosphere over rothera, antarctica (68°s, 68°w). *Journal of Geophysical Research*, 115(D18). Retrieved from <https://doi.org/10.1029/2009jd013617> doi: 10.1029/2009jd013617
- 659
- 660
- 661
- 662 Bremer, J., Schminder, R., Greisiger, K., Hoffmann, P., Kürschner, D., & Singer, W. (1997, March). Solar cycle dependence and long-term trends in the wind field of the mesosphere/lower thermosphere. *Journal of Atmospheric and Solar-Terrestrial Physics*, 59(5), 497–509. Retrieved from [https://doi.org/10.1016/s1364-6826\(96\)00032-6](https://doi.org/10.1016/s1364-6826(96)00032-6) doi: 10.1016/s1364-6826(96)00032-6
- 663
- 664
- 665
- 666
- 667 Chapman, S., & Lindzen, R. S. (1970). *Atmospheric tides* (1970th ed.). Dordrecht, Netherlands: Springer.
- 668
- 669 Chiodo, G., Marsh, D. R., Garcia-Herrera, R., Calvo, N., & García, J. A. (2014, June). On the detection of the solar signal in the tropical stratosphere. *Atmospheric Chemistry and Physics*, 14(11), 5251–5269. Retrieved from <https://doi.org/10.5194/acp-14-5251-2014> doi: 10.5194/acp-14-5251-2014
- 670
- 671
- 672
- 673 Conte, J. F., Chau, J. L., Stober, G., Pedatella, N., Maute, A., Hoffmann, P., ... Murphy, D. J. (2017, July). Climatology of semidiurnal lunar and solar tides at middle and high latitudes: Interhemispheric comparison. *Journal of Geophysical Research: Space Physics*, 122(7), 7750–7760. Retrieved from <https://doi.org/10.1002/2017ja024396> doi: 10.1002/2017ja024396
- 674
- 675
- 676
- 677
- 678 Davis, R. N., Du, J., Smith, A. K., Ward, W. E., & Mitchell, N. J. (2013, September). The diurnal and semidiurnal tides over ascension island (° s, 14° w) and their interaction with the stratospheric quasi-biennial oscillation: studies with meteor radar, eCMAM and WACCM. *Atmospheric Chemistry and Physics*, 13(18), 9543–9564. Retrieved from <https://doi.org/10.5194/acp-13-9543-2013> doi: 10.5194/acp-13-9543-2013
- 679
- 680
- 681
- 682
- 683
- 684 Day, K. A., Taylor, M. J., & Mitchell, N. J. (2012, February). Mean winds, temperatures and the 16- and 5-day planetary waves in the mesosphere and lower thermosphere over bear lake observatory (42° n, 111° w). *Atmospheric Chemistry and Physics*, 12(3), 1571–1585. Retrieved from <https://doi.org/10.5194/acp-12-1571-2012> doi: 10.5194/acp-12-1571-2012
- 685
- 686
- 687
- 688
- 689 Dempsey, S. M., Hindley, N. P., Moffat-Griffin, T., Wright, C. J., Smith, A. K., Du, J., & Mitchell, N. J. (2021, January). Winds and tides of the antarctic mesosphere and lower thermosphere: One year of meteor-radar observations over rothera (68°s, 68°w) and comparisons with WACCM and eCMAM. *Journal of Atmospheric and Solar-Terrestrial Physics*, 212, 105510. Retrieved from <https://doi.org/10.1016/j.jastp.2020.105510> doi: 10.1016/j.jastp.2020.105510
- 690
- 691
- 692
- 693
- 694
- 695

- 696 Dhadly, M. S., Emmert, J. T., Drob, D. P., McCormack, J. P., & Nijewski, R. J.
697 (2018, August). Short-term and interannual variations of migrating diurnal
698 and semidiurnal tides in the mesosphere and lower thermosphere. *Journal*
699 *of Geophysical Research: Space Physics*, *123*(8), 7106–7123. Retrieved from
700 <https://doi.org/10.1029/2018ja025748> doi: 10.1029/2018ja025748
- 701 Fiedler, J., Baumgarten, G., & von Cossart, G. (2005, June). Mean diurnal varia-
702 tions of noctilucent clouds during 7 years of lidar observations at ALOMAR.
703 *Annales Geophysicae*, *23*(4), 1175–1181. Retrieved from [https://doi.org/](https://doi.org/10.5194/angeo-23-1175-2005)
704 [10.5194/angeo-23-1175-2005](https://doi.org/10.5194/angeo-23-1175-2005) doi: 10.5194/angeo-23-1175-2005
- 705 Forbes, J. M. (1982, July). Atmospheric tides: 1. model description and results
706 for the solar diurnal component. *Journal of Geophysical Research: Space*
707 *Physics*, *87*(A7), 5222–5240. Retrieved from [https://doi.org/10.1029/](https://doi.org/10.1029/ja087ia07p05222)
708 [ja087ia07p05222](https://doi.org/10.1029/ja087ia07p05222) doi: 10.1029/ja087ia07p05222
- 709 Forbes, J. M., Zhang, X., Palo, S., Russell, J., Mertens, C. J., & Mlynczak, M.
710 (2008, February). Tidal variability in the ionospheric dynamo region. *Journal*
711 *of Geophysical Research: Space Physics*, *113*(A2), n/a–n/a. Retrieved from
712 <https://doi.org/10.1029/2007ja012737> doi: 10.1029/2007ja012737
- 713 Fritts, D. C., & Alexander, M. J. (2003, March). Gravity wave dynamics and ef-
714 fects in the middle atmosphere. *Reviews of Geophysics*, *41*(1). Retrieved from
715 <https://doi.org/10.1029/2001rg000106> doi: 10.1029/2001rg000106
- 716 Gan, Q., Du, J., Fomichev, V. I., Ward, W. E., Beagley, S. R., Zhang, S., & Yue,
717 J. (2017, April). Temperature responses to the 11 year solar cycle in the
718 mesosphere from the 31 year (1979–2010) extended canadian middle atmo-
719 sphere model simulations and a comparison with the 14 year (2002–2015)
720 TIMED/SABER observations. *Journal of Geophysical Research: Space*
721 *Physics*, *122*(4), 4801–4818. Retrieved from [https://doi.org/10.1002/](https://doi.org/10.1002/2016ja023564)
722 [2016ja023564](https://doi.org/10.1002/2016ja023564) doi: 10.1002/2016ja023564
- 723 Guharay, A., Batista, P., & Andrioli, V. (2019, October). Investigation of solar
724 cycle dependence of the tides in the low latitude MLT using meteor radar
725 observations. *Journal of Atmospheric and Solar-Terrestrial Physics*, *193*,
726 105083. Retrieved from <https://doi.org/10.1016/j.jastp.2019.105083>
727 doi: 10.1016/j.jastp.2019.105083
- 728 Hagan, M. E. (1996, September). Comparative effects of migrating solar sources
729 on tidal signatures in the middle and upper atmosphere. *Journal of Geophysi-
730 cal Research: Atmospheres*, *101*(D16), 21213–21222. Retrieved from [https://](https://doi.org/10.1029/96jd01374)
731 doi.org/10.1029/96jd01374 doi: 10.1029/96jd01374
- 732 Hagan, M. E., & Forbes, J. M. (2002, December). Migrating and nonmigrat-
733 ing diurnal tides in the middle and upper atmosphere excited by tropo-
734 spheric latent heat release. *Journal of Geophysical Research: Atmospheres*,
735 *107*(D24). Retrieved from <https://doi.org/10.1029/2001jd001236> doi:
736 [10.1029/2001jd001236](https://doi.org/10.1029/2001jd001236)
- 737 Hagan, M. E., Maute, A., & Roble, R. G. (2009, January). Tropospheric tidal ef-
738 fects on the middle and upper atmosphere. *Journal of Geophysical Research:*
739 *Space Physics*, *114*(A1), n/a–n/a. Retrieved from [https://doi.org/10.1029/](https://doi.org/10.1029/2008ja013637)
740 [2008ja013637](https://doi.org/10.1029/2008ja013637) doi: 10.1029/2008ja013637
- 741 Hagan, M. E., Roble, R. G., & Hackney, J. (2001, July). Migrating thermospheric
742 tides. *Journal of Geophysical Research: Space Physics*, *106*(A7), 12739–
743 12752. Retrieved from <https://doi.org/10.1029/2000ja000344> doi:
744 [10.1029/2000ja000344](https://doi.org/10.1029/2000ja000344)
- 745 Hibbins, R., Espy, P., Jarvis, M., Riggin, D., & Fritts, D. (2007, April). A clima-
746 tology of tides and gravity wave variance in the MLT above Rothera, Antarc-
747 tica obtained by MF radar. *Journal of Atmospheric and Solar-Terrestrial*
748 *Physics*, *69*(4-5), 578–588. Retrieved from [https://doi.org/10.1016/](https://doi.org/10.1016/j.jastp.2006.10.009)
749 [j.jastp.2006.10.009](https://doi.org/10.1016/j.jastp.2006.10.009) doi: 10.1016/j.jastp.2006.10.009
- 750 Hibbins, R., Marsh, O., McDonald, A., & Jarvis, M. (2010, June). Interannual vari-

- 751 ability of the $s=1$ and $s=2$ components of the semidiurnal tide in the antarctic
 752 MLT. *Journal of Atmospheric and Solar-Terrestrial Physics*, 72(9-10), 794–
 753 800. Retrieved from <https://doi.org/10.1016/j.jastp.2010.03.026> doi:
 754 10.1016/j.jastp.2010.03.026
- 755 Hindley, N. P., Cobbett, N., Fritts, D. C., Janchez, D., Mitchell, N. J., Moffat-
 756 Griffin, T., ... Wright, C. J. (2021, December). Radar observations of winds,
 757 waves and tides in the mesosphere and lower thermosphere over south georgia
 758 island (54°s, 36°w) and comparison to WACCM simulations. *ACP*. Retrieved
 759 from <https://doi.org/10.5194/acp-2021-981> doi: 10.5194/acp-2021-981
- 760 Hines, C., Adams, G., Brosnahan, J., Djuth, F., Sulzer, M., Tepley, C., & Baelen,
 761 J. V. (1993, March). Multi-instrument observations of mesospheric motions
 762 over arecibo: comparisons and interpretations. *Journal of Atmospheric
 763 and Terrestrial Physics*, 55(3), 241–287. Retrieved from [https://doi.org/
 764 10.1016/0021-9169\(93\)90069-b](https://doi.org/10.1016/0021-9169(93)90069-b) doi: 10.1016/0021-9169(93)90069-b
- 765 Hocking, W., Fuller, B., & Vandeppeer, B. (2001, January). Real-time determi-
 766 nation of meteor-related parameters utilizing modern digital technology.
 767 *Journal of Atmospheric and Solar-Terrestrial Physics*, 63(2-3), 155–169.
 768 Retrieved from [https://doi.org/10.1016/s1364-6826\(00\)00138-3](https://doi.org/10.1016/s1364-6826(00)00138-3) doi:
 769 10.1016/s1364-6826(00)00138-3
- 770 Immel, T. J., Sagawa, E., England, S. L., Henderson, S. B., Hagan, M. E., Mende,
 771 S. B., ... Paxton, L. J. (2006). Control of equatorial ionospheric morphology
 772 by atmospheric tides. *Geophysical Research Letters*, 33(15). Retrieved from
 773 <https://doi.org/10.1029/2006gl026161> doi: 10.1029/2006gl026161
- 774 Jones, M., Forbes, J. M., Hagan, M. E., & Maute, A. (2013, May). Non-migrating
 775 tides in the ionosphere-thermosphere: In situ versus tropospheric sources.
 776 *Journal of Geophysical Research: Space Physics*, 118(5), 2438–2451. Retrieved
 777 from <https://doi.org/10.1002/jgra.50257> doi: 10.1002/jgra.50257
- 778 Kalnins, A. (2018, May). Multicollinearity: How common factors cause type 1 errors
 779 in multivariate regression. *Strategic Management Journal*, 39(8), 2362–2385.
 780 Retrieved from <https://doi.org/10.1002/smj.2783> doi: 10.1002/smj.2783
- 781 Kumari, K., & Oberheide, J. (2020, March). QBO, ENSO, and solar cycle effects
 782 in short-term nonmigrating tidal variability on planetary wave timescales from
 783 SABER—an information-theoretic approach. *Journal of Geophysical Re-
 784 search: Atmospheres*, 125(6). Retrieved from [https://doi.org/10.1029/
 785 2019jd031910](https://doi.org/10.1029/2019jd031910) doi: 10.1029/2019jd031910
- 786 Laskar, F. I., Chau, J. L., Stober, G., Hoffmann, P., Hall, C. M., & Tsutsumi, M.
 787 (2016, May). Quasi-biennial oscillation modulation of the middle- and high-
 788 latitude mesospheric semidiurnal tides during august-september. *Journal of
 789 Geophysical Research: Space Physics*, 121(5), 4869–4879. Retrieved from
 790 <https://doi.org/10.1002/2015ja022065> doi: 10.1002/2015ja022065
- 791 Lee, D. Y., Petersen, M. R., & Lin, W. (2019, December). The southern annular
 792 mode and southern ocean surface westerly winds in e3sm. *Earth and Space
 793 Science*, 6(12), 2624–2643. Retrieved from [https://doi.org/10.1029/
 794 2019ea000663](https://doi.org/10.1029/2019ea000663) doi: 10.1029/2019ea000663
- 795 Lieberman, R. S., Riggins, D. M., Ortland, D. A., Nesbitt, S. W., & Vincent,
 796 R. A. (2007, October). Variability of mesospheric diurnal tides and tropo-
 797 spheric diurnal heating during 1997–1998. *Journal of Geophysical Research*,
 798 112(D20). Retrieved from <https://doi.org/10.1029/2007jd008578> doi:
 799 10.1029/2007jd008578
- 800 Liu, H., Sun, Y.-Y., Miyoshi, Y., & Jin, H. (2017, May). ENSO effects on MLT di-
 801 urnal tides: A 21 year reanalysis data-driven GAIA model simulation. *Journal
 802 of Geophysical Research: Space Physics*, 122(5), 5539–5549. Retrieved from
 803 <https://doi.org/10.1002/2017ja024011> doi: 10.1002/2017ja024011
- 804 Liu, H.-L. (2016, September). Variability and predictability of the space envi-
 805 ronment as related to lower atmosphere forcing. *Space Weather*, 14(9),

- 806 634–658. Retrieved from <https://doi.org/10.1002/2016sw001450> doi:
807 10.1002/2016sw001450
- 808 Manson, A. H., Meek, C. E., Hall, C. M., Nozawa, S., Mitchell, N. J., Pancheva,
809 D., . . . Hoffmann, P. (2004, January). Mesopause dynamics from the scan-
810 dinavian triangle of radars within the PSMOS-DATAR project. *Annales*
811 *Geophysicae*, *22*(2), 367–386. Retrieved from [https://doi.org/10.5194/](https://doi.org/10.5194/angeo-22-367-2004)
812 [angeo-22-367-2004](https://doi.org/10.5194/angeo-22-367-2004) doi: 10.5194/angeo-22-367-2004
- 813 Marshall, G. J. (2003, December). Trends in the southern annular mode from obser-
814 vations and reanalyses. *Journal of Climate*, *16*(24), 4134–4143. Retrieved from
815 [https://doi.org/10.1175/1520-0442\(2003\)016<4134:titsam>2.0.co;2](https://doi.org/10.1175/1520-0442(2003)016<4134:titsam>2.0.co;2)
816 doi: 10.1175/1520-0442(2003)016(4134:titsam)2.0.co;2
- 817 Marshall, G. J. (2018, Mar). *Marshall southern annular mode (sam) index (station-*
818 *based)*. Retrieved from [https://climatedataguide.ucar.edu/climate](https://climatedataguide.ucar.edu/climate-data/marshall-southern-annular-mode-sam-index-station-based)
819 [-data/marshall-southern-annular-mode-sam-index-station-based](https://climatedataguide.ucar.edu/climate-data/marshall-southern-annular-mode-sam-index-station-based)
- 820 Mayr, H. G., Mengel, J. G., Talaat, E. R., Porter, H. S., & Chan, K. L. (2003,
821 August). Non-migrating diurnal tides generated with planetary waves in
822 the mesosphere. *Geophysical Research Letters*, *30*(16). Retrieved from
823 <https://doi.org/10.1029/2003gl017877> doi: 10.1029/2003gl017877
- 824 McLandress, C., & Ward, W. E. (1994). Tidal/gravity wave interactions and
825 their influence on the large-scale dynamics of the middle atmosphere: Model
826 results. *Journal of Geophysical Research*, *99*(D4), 8139. Retrieved from
827 <https://doi.org/10.1029/94jd00486> doi: 10.1029/94jd00486
- 828 Merzlyakov, E., Murphy, D., Vincent, R., & Portnyagin, Y. (2009, January). Long-
829 term tendencies in the MLT prevailing winds and tides over antarctica as
830 observed by radars at molodezhnaya, mawson and davis. *Journal of Atmo-*
831 *spheric and Solar-Terrestrial Physics*, *71*(1), 21–32. Retrieved from [https://](https://doi.org/10.1016/j.jastp.2008.09.024)
832 doi.org/10.1016/j.jastp.2008.09.024 doi: 10.1016/j.jastp.2008.09.024
- 833 Mitchell, N., & Beldon, C. (2009, June). Gravity waves in the mesopause re-
834 gion observed by meteor radar: 1. a simple measurement technique. *Jour-*
835 *nal of Atmospheric and Solar-Terrestrial Physics*, *71*(8-9), 866–874. Re-
836 trieved from <https://doi.org/10.1016/j.jastp.2009.03.011> doi:
837 10.1016/j.jastp.2009.03.011
- 838 Mitchell, N. J. (2002). Mean winds and tides in the arctic mesosphere and lower
839 thermosphere. *Journal of Geophysical Research*, *107*(A1). Retrieved from
840 <https://doi.org/10.1029/2001ja900127> doi: 10.1029/2001ja900127
- 841 Mthembu, S., Sivakumar, V., Mitchell, N., & Malinga, S. (2013, September). Studies
842 on planetary waves and tide interaction in the mesosphere/lower thermo-
843 sphere region using meteor RADAR data from rothera (68°s, 68°w), antar-
844 ctica. *Journal of Atmospheric and Solar-Terrestrial Physics*, *102*, 59–70.
845 Retrieved from <https://doi.org/10.1016/j.jastp.2013.04.012> doi:
846 10.1016/j.jastp.2013.04.012
- 847 Murphy, D. J. (2003). Observations of a nonmigrating component of the semidiur-
848 nal tide over antarctica. *Journal of Geophysical Research*, *108*(D8). Retrieved
849 from <https://doi.org/10.1029/2002jd003077> doi: 10.1029/2002jd003077
- 850 Namboothiri, S., Manson, A., & Meek, C. (1993, August). Variations of
851 mean winds and tides in the upper middle atmosphere over a solar cycle,
852 saskatoon, canada, 52°n, 107°w. *Journal of Atmospheric and Terrestrial*
853 *Physics*, *55*(10), 1325–1334. Retrieved from [https://doi.org/10.1016/](https://doi.org/10.1016/0021-9169(93)90101-4)
854 [0021-9169\(93\)90101-4](https://doi.org/10.1016/0021-9169(93)90101-4) doi: 10.1016/0021-9169(93)90101-4
- 855 Nischal, N., Oberheide, J., Mlynczak, M. G., Marsh, D. R., & Gan, Q. (2019,
856 March). Solar cycle variability of nonmigrating tides in the 5.3 and 15 μ m
857 infrared cooling of the thermosphere (100 – 150 km) from SABER. *Journal*
858 *of Geophysical Research: Space Physics*, *124*(3), 2338–2356. Retrieved from
859 <https://doi.org/10.1029/2018ja026356> doi: 10.1029/2018ja026356
- 860 Noble, P., Hindley, N., Wright, C., Cullens, C., England, S., Pedatella, N., . . .

- 861 Moffat-Griffin, T. (2022, May). Interannual variability of winds in the antarctic
862 mesosphere and lower thermosphere over rothera (67° s, 68° w) in radar
863 observations and WACCM-X. *Atmospheric Chemistry and Physics*. Retrieved
864 from <https://doi.org/10.5194/acp-2022-150> doi: 10.5194/acp-2022-150
- 865 Oberheide, J., Forbes, J. M., Häusler, K., Wu, Q., & Bruinsma, S. L. (2009, Jan-
866 uary). Tropospheric tides from 80 to 400 km: Propagation, interannual vari-
867 ability, and solar cycle effects. *Journal of Geophysical Research: Atmospheres*,
868 *114*(D1). Retrieved from <https://doi.org/10.1029/2009jd012388> doi:
869 10.1029/2009jd012388
- 870 Pancheva, D., Mitchell, N., Middleton, H., & Muller, H. (2003, January). Vari-
871 ability of the semidiurnal tide due to fluctuations in solar activity and total
872 ozone. *Journal of Atmospheric and Solar-Terrestrial Physics*, *65*(1), 1–19.
873 Retrieved from [https://doi.org/10.1016/s1364-6826\(02\)00084-6](https://doi.org/10.1016/s1364-6826(02)00084-6) doi:
874 10.1016/s1364-6826(02)00084-6
- 875 Pancheva, D., Mukhtarov, P., & Andonov, B. (2009, February). Global structure,
876 seasonal and interannual variability of the migrating semidiurnal tide seen in
877 the SABER/TIMED temperatures (2002–2007). *Annales Geophysicae*, *27*(2),
878 687–703. Retrieved from <https://doi.org/10.5194/angeo-27-687-2009>
879 doi: 10.5194/angeo-27-687-2009
- 880 Pedatella, N. M., & Liu, H.-L. (2012, October). Tidal variability in the mesosphere
881 and lower thermosphere due to the el niño-southern oscillation. *Geophys-
882 ical Research Letters*, *39*(19), n/a–n/a. Retrieved from [https://doi.org/
883 10.1029/2012gl053383](https://doi.org/10.1029/2012gl053383) doi: 10.1029/2012gl053383
- 884 Ramesh, K., Smith, A. K., Garcia, R. R., Marsh, D. R., Sridharan, S., & Ku-
885 mar, K. K. (2020, December). Long-term variability and tendencies
886 in migrating diurnal tide from WACCM6 simulations during 1850–2014.
887 *Journal of Geophysical Research: Atmospheres*, *125*(23). Retrieved from
888 <https://doi.org/10.1029/2020jd033644> doi: 10.1029/2020jd033644
- 889 Sandford, D., Mitchell, N., Vincent, R., & Murphy, D. (2007, December). The lu-
890 nar tides in the antarctic mesosphere and lower thermosphere. *Journal of At-
891 mospheric and Solar-Terrestrial Physics*, *69*(17-18), 2219–2237. Retrieved from
892 <https://doi.org/10.1016/j.jastp.2007.04.010> doi: 10.1016/j.jastp.2007
893 .04.010
- 894 Sandford, D. J., Beldon, C. L., Hibbins, R. E., & Mitchell, N. J. (2010, November).
895 Dynamics of the antarctic and arctic mesosphere and lower thermosphere –
896 part 1: Mean winds. *Atmospheric Chemistry and Physics*, *10*(21), 10273–
897 10289. Retrieved from <https://doi.org/10.5194/acp-10-10273-2010> doi:
898 10.5194/acp-10-10273-2010
- 899 Sassi, F. (2004). Effect of el niño–southern oscillation on the dynamical, thermal,
900 and chemical structure of the middle atmosphere. *Journal of Geophysical Re-
901 search*, *109*(D17). Retrieved from <https://doi.org/10.1029/2003jd004434>
902 doi: 10.1029/2003jd004434
- 903 Smith, A. K. (2012, June). Global dynamics of the MLT. *Surveys in Geo-
904 physics*, *33*(6), 1177–1230. Retrieved from [https://doi.org/10.1007/
905 s10712-012-9196-9](https://doi.org/10.1007/s10712-012-9196-9) doi: 10.1007/s10712-012-9196-9
- 906 Sobhkhiz-Miandehi, S., Yamazaki, Y., Arras, C., Miyoshi, Y., & Shinagawa, H.
907 (2022, June). Comparison of the tidal signatures in sporadic e and ver-
908 tical ion convergence rate, using FORMOSAT-3/COSMIC radio occul-
909 tation observations and GAIA model. *Earth, Planets and Space*, *74*(1).
910 Retrieved from <https://doi.org/10.1186/s40623-022-01637-y> doi:
911 10.1186/s40623-022-01637-y
- 912 Song, B.-G., Song, I.-S., Chun, H.-Y., Lee, C., Kam, H., Kim, Y. H., . . . Mitchell,
913 N. J. (2021, May). Activities of small-scale gravity waves in the upper meso-
914 sphere observed from meteor radar at king sejong station, antarctica (62.22°s,
915 58.78°w) and their potential sources. *Journal of Geophysical Research: Atmo-*

- 916 *spheres*, 126(10). Retrieved from <https://doi.org/10.1029/2021jd034528>
 917 doi: 10.1029/2021jd034528
- 918 Sprenger, K., & Schindler, R. (1969, January). Solar cycle dependence of winds in
 919 the lower ionosphere. *Journal of Atmospheric and Terrestrial Physics*, 31(1),
 920 217–221. Retrieved from [https://doi.org/10.1016/0021-9169\(69\)90100-7](https://doi.org/10.1016/0021-9169(69)90100-7)
 921 doi: 10.1016/0021-9169(69)90100-7
- 922 Stober, G., Janches, D., Matthias, V., Fritts, D., Marino, J., Moffat-Griffin, T., ...
 923 Palo, S. (2021, January). Seasonal evolution of winds, atmospheric tides,
 924 and reynolds stress components in the southern hemisphere mesosphere–lower
 925 thermosphere in 2019. *Annales Geophysicae*, 39(1), 1–29. Retrieved from
 926 <https://doi.org/10.5194/angeo-39-1-2021> doi: 10.5194/angeo-39-1-2021
- 927 Stober, G., Kuchar, A., Pokhotelov, D., Liu, H., Liu, H.-L., Schmidt, H., ...
 928 Mitchell, N. (2021, September). Interhemispheric differences of meso-
 929 sphere–lower thermosphere winds and tides investigated from three whole-
 930 atmosphere models and meteor radar observations. *Atmospheric Chem-
 931 istry and Physics*, 21(18), 13855–13902. Retrieved from <https://doi.org/10.5194/acp-21-13855-2021>
 932 doi: 10.5194/acp-21-13855-2021
- 933 Sundararajan, S. (2020, June). Equatorial upper mesospheric mean winds and tidal
 934 response to strong el niño and la niña. *Journal of Atmospheric and Solar-
 935 Terrestrial Physics*, 202, 105270. Retrieved from <https://doi.org/10.1016/j.jastp.2020.105270>
 936 doi: 10.1016/j.jastp.2020.105270
- 937 Trenberth, K. (2018, Jan). *Nino sst indices (nino 1 2, 3, 3.4, 4; oni and tni)*.
 938 National Center for Atmospheric Research. Retrieved from [https://
 939 climatedataguide.ucar.edu/climate-data/nino-sst-indices-nino-12
 940 -3-34-4-oni-and-tni](https://climatedataguide.ucar.edu/climate-data/nino-sst-indices-nino-12-3-34-4-oni-and-tni)
- 941 Trenberth, K. E. (2002). Evolution of el niño–southern oscillation and global
 942 atmospheric surface temperatures. *Journal of Geophysical Research*,
 943 107(D8). Retrieved from <https://doi.org/10.1029/2000jd000298> doi:
 944 10.1029/2000jd000298
- 945 Vadas, S. L., Liu, H.-L., & Lieberman, R. S. (2014, September). Numerical
 946 modeling of the global changes to the thermosphere and ionosphere from
 947 the dissipation of gravity waves from deep convection. *Journal of Geo-
 948 physical Research: Space Physics*, 119(9), 7762–7793. Retrieved from
 949 <https://doi.org/10.1002/2014ja020280> doi: 10.1002/2014ja020280
- 950 Vitharana, A., Zhu, X., Du, J., Oberheide, J., & Ward, W. E. (2019, August). Sta-
 951 tistical modeling of tidal weather in the mesosphere and lower thermosphere.
 952 *Journal of Geophysical Research: Atmospheres*, 124(16), 9011–9027. Retrieved
 953 from <https://doi.org/10.1029/2019jd030573> doi: 10.1029/2019jd030573
- 954 Webster, A. (2012). *Introductory regression analysis : With computer application for
 955 business and economics*. London: Taylor & Francis Group.
- 956 Wilhelm, S., Stober, G., & Chau, J. L. (2017, July). A comparison of 11-year meso-
 957 spheric and lower thermospheric winds determined by meteor and MF radar
 958 at 69 N. *Annales Geophysicae*, 35(4), 893–906. Retrieved from [https://
 959 doi.org/10.5194/angeo-35-893-2017](https://doi.org/10.5194/angeo-35-893-2017) doi: 10.5194/angeo-35-893-2017
- 960 Yiğit, E., & Medvedev, A. S. (2015, February). Internal wave coupling processes in
 961 earth’s atmosphere. *Advances in Space Research*, 55(4), 983–1003. Retrieved
 962 from <https://doi.org/10.1016/j.asr.2014.11.020> doi: 10.1016/j.asr.2014
 963 .11.020
- 964 Yiğit, E., Medvedev, A. S., & Ern, M. (2021, February). Effects of latitude-
 965 dependent gravity wave source variations on the middle and upper atmosphere.
 966 *Frontiers in Astronomy and Space Sciences*, 7. Retrieved from [https://
 967 doi.org/10.3389/fspas.2020.614018](https://doi.org/10.3389/fspas.2020.614018) doi: 10.3389/fspas.2020.614018